Co-generation of hydroxyl and sulfate radicals via homogeneous and heterogeneous bi-catalysis with the EO-PS-EF tri-coupling system for efficient removal of refractory organic pollutants

Supplementary Materials

Co-generation of hydroxyl and sulfate radicals via homogeneous and heterogeneous bi-catalysis with the EO-PS-EF tri-coupling system for efficient removal of refractory organic pollutants

Wanlin Yang[a], Zejun Deng[a,*], Libin Liu[a], Kechao Zhou[a], Sharel P. E[b], Lingcong Meng[c], Li Ma[a,*], Qiuping Wei[a,*]

[a]School of Materials Science and Engineering, State Key Laboratory of Powder Metallurgy, Central South University, Changsha 410083, P.R. China

[b]School of Engineering, University of Edinburgh, Edinburgh, EH9 3DW

[c]School of Chemistry, University of Edinburgh, David Brewster Rd, Edinburgh EH9 3FJ

[*]Corresponding authors:

E-mail address: zejun.deng@csu.edu.cn (Dr. Z. Deng); marycsupm@csu.edu.cn (Dr. L. Ma); qiupwei@csu.edu.cn (Dr. Q. Wei).

Table S1

Parameters of HPLC-UV methods for TC, ATZ and 2,4-D analysis.

Parameters	TC	ATZ	2,4-D
UV detection wavelength (nm)	358	225	282
flow rate (mL min^{-1})	0.35	0.8	0.35
injection volume (µL)	20	10	10
analysis time (min)	14	10	25
mobile phase	10:90 (v/v) acetonitrile/0.1% formic acid mixture	70:30 (v/v) methanol/ultra pure water mixture	60:40 (v/v) acetonitrile/2% acetic acid mixture

Table S2

Physicochemical information on refractory organic pollutants used in this work.

Commercial name	Chemical structure	Chemical formula	Molar weight	CAS number
Tetracycline	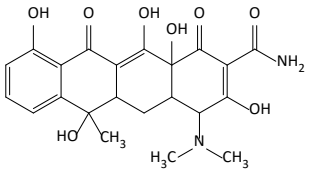	$C_{22}H_{24}N_2O_8$	444.45	60-54-8
Atrazine	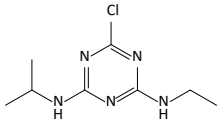	$C_8H_{14}ClN_5$	215.68	1912-24-9
2,4-Dichloro-phenoxyacetic acid	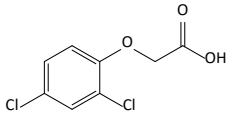	$C_8H_6Cl_2O_3$	221.04	94-75-7
Orange G	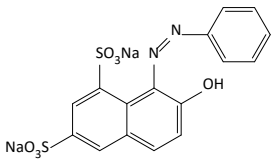	$C_{16}H_{10}N_2Na_2O_7S_2$	452.37	1936-15-8
Reactive Blue 19	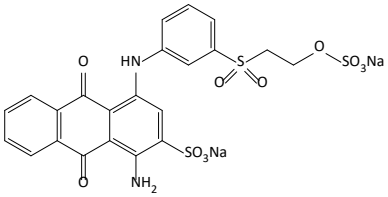	$C_{22}H_{16}N_2Na_2O_{11}S_3$	626.54	2580-78-1

LC-MS detection information

Instrument Model: Agilent LC1290-QQQ-6470

Chromatographic column: ACE, UltraCore C18, 2.1×75 mm, 2.5 μm

Column temperature: 40 °C Mobile phase: A (acetonitrile) B (0.1% formic acid)

Flow velocity: 0.35 mL min^{-1} Sample size: 20 μL

Auto-sampler temperature: 25 °C

Table S3

The mobile phase ratios are shown in the following table.

Time (min)	Flow (mL min^{-1})	A conc. (%)	B conc. (%)
0	0.35	10	90
10	0.35	90	10
14	0.35	90	10

Mass Spectrometry Acquisition Parameters:

Type of ion source: ESI Pattern: MS2 Scan

Polarity: positive mode Scan range: m/z 30-600

Dry gas temperature: 150 °C Dry gas flow velocity: 12 L min^{-1}

Sheath gas temperature: 350 °C Sheath gas flow velocity: 12 L min^{-1}

Nebulizer pressure: 30 Psi Capillary voltage: 3500 V

Scan time: 300 ms Fragmentor: 135 V Scan step: 0.1 amu

Data processing method:

Integrator: Agile 2

Mass spectrum background deduction method: The average mass spectrum within the specified retention time period at the beginning of the sample analysis were selected as the background.

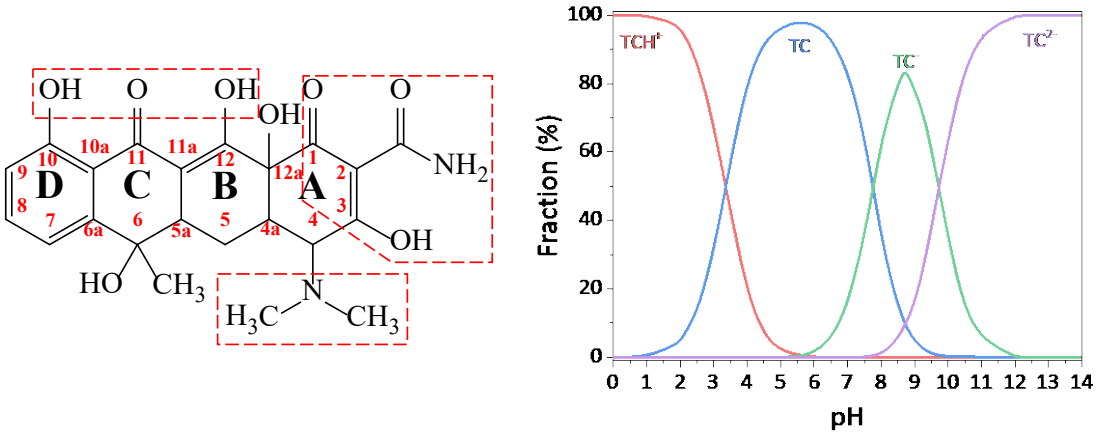

Fig. S1. (a) Molecular structure of TC on a planar view and (b) speciation under different pH. pK_{a1} was due to the protonation of the oxygen bond at the C3 position. pK_{a2} was caused by the protonation of oxygen bonds at the C10 and C12 positions. pK_{a3} was resulted from the protonation of the dimethylamine functional group at the C4 position.

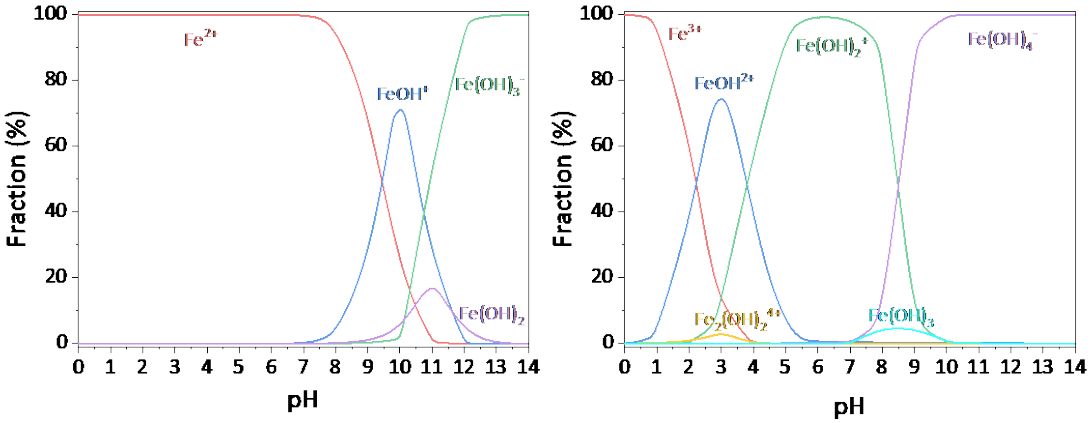

Fig. S2. Distribution of the (a) Fe(II) and (b) Fe(III) as a function of pH variation.

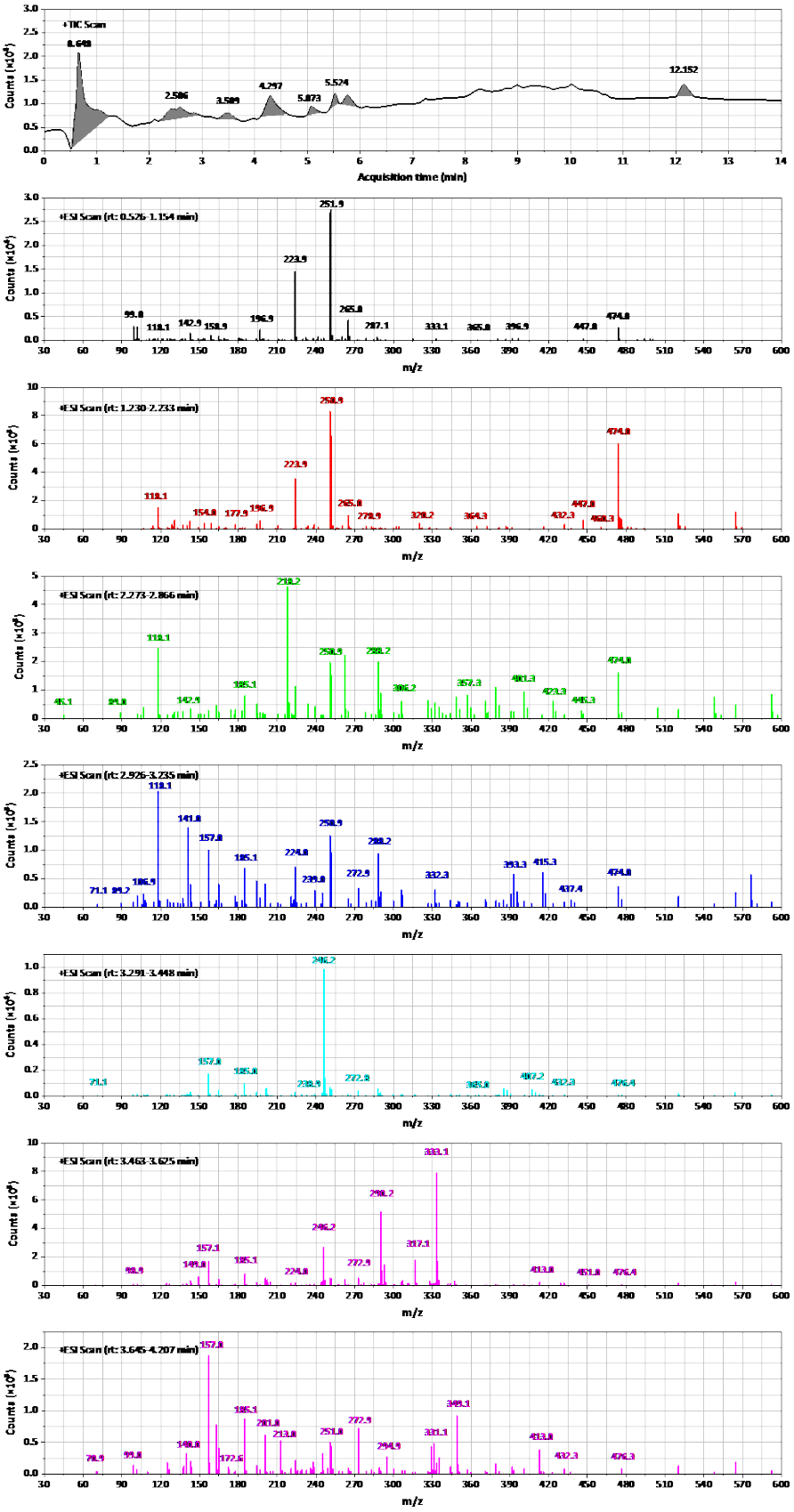
+TIC Scan
8.648
2.586
3.589
4.297
5.073
5.524
12.152
Counts (x10⁶)
Acquisition time (min)
+ESI Scan (rt: 0.526-1.154 min)
+ESI Scan (rt: 1.230-2.233 min)
+ESI Scan (rt: 2.273-2.866 min)
+ESI Scan (rt: 2.926-3.235 min)
+ESI Scan (rt: 3.291-3.448 min)
+ESI Scan (rt: 3.463-3.625 min)
+ESI Scan (rt: 3.645-4.207 min)
m/z

50

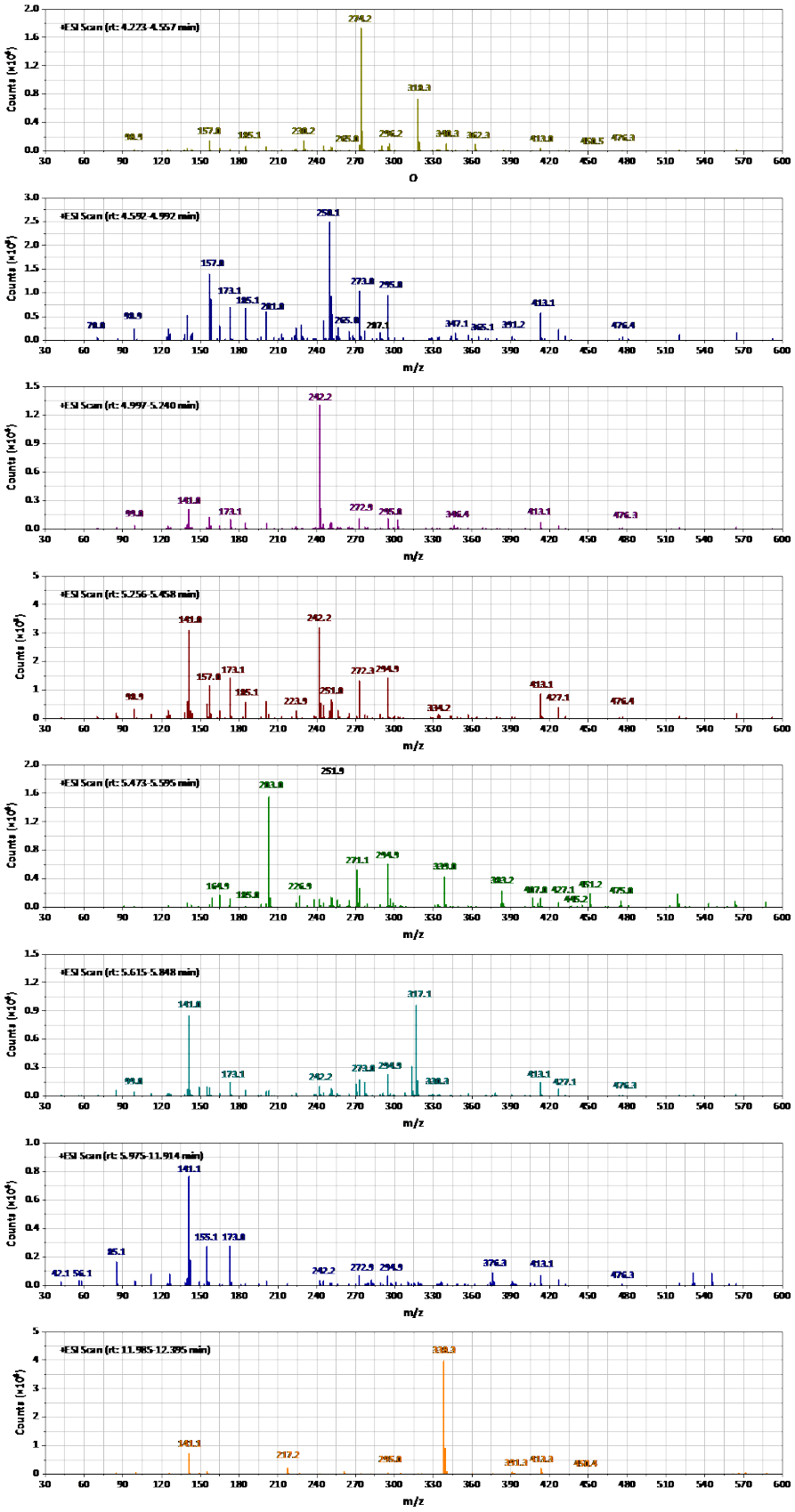

Fig. S3. Total ions chromatogram and mass spectra with different residence times of TC degradation in the EO-PS-EF system.

Table S4

Details of reaction intermediates identified for degraded TC by LC-MS analysis.

No.	Chemical name	Chemical structure	Chemical formula	Molecular weight	m/z
1	4-(dimethylamino)-2,6,10,11a,12a-pentahydroxy-6-methyl-1,3,11,12-tetraoxo-1,2,3,4,4a,5,5a,6,11,11a,12,12a-dodecahydrotetracene-2-carboxamide	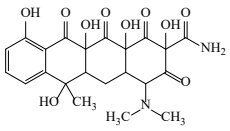	$C_{22}H_{24}N_2O_{10}$	476.44	476
2	3,6,10,11a,12a-pentahydroxy-6-methyl-4-(N-methylformamido)-1,11,12-trioxo-1,4,4a,5,5a,6,11,11a,12,12a-decahydrotetracene-2-carboxamide	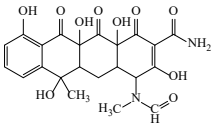	$C_{22}H_{22}N_2O_{10}$	474.42	474
3	4-(dimethylamino)-3,6,10,11a,12a-pentahydroxy-6-methyl-1,11,12-trioxo-1,4,4a,5,5a,6,11,11a,12,12a-decahydrotetracene-2-carboxamide	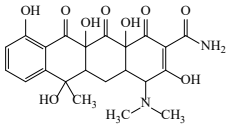	$C_{22}H_{24}N_2O_9$	460.44	460
4	2,6,10,11a,12a-pentahydroxy-6-methyl-1,3,4,11,12-pentaoxo-1,2,3,4,4a,5,5a,6,11,11a,12,12a-dodecahydrotetracene-2-carboxamide	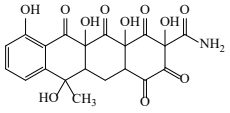	$C_{20}H_{17}NO_{11}$	447.35	447
5	3,6,10,11a,12a-pentahydroxy-6-methyl-1,4,11,12-tetraoxo-1,4,4a,5,5a,6,11,11a,12,12a-decahydrotetracene-2-carboxamide	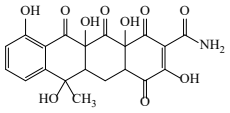	$C_{20}H_{17}NO_{10}$	431.35	432
6	4-amino-3,6,10,12,12a-pentahydroxy-6-methyl-1,11-dioxo-1,4,4a,5,5a,6,11,12a-octahydrotetracene-2-carboxamide	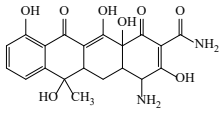	$C_{20}H_{20}N_2O_8$	416.39	416
7	2,3,4a,5a,7,11-hexahydroxy-11-methyl-2,3,11,11a,12,12a-hexahydrotetracene-1,4,5,6(4a,5a)-tetraone	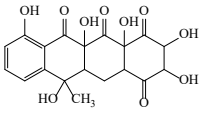	$C_{19}H_{18}O_{10}$	406.34	407
8	4-(dimethylamino)-3,6,10,12,12a-pentahydroxy-6-methyl-4a,5a,6,12a-tetrahydrotetracene-1,11(4*H*,5*H*)-dione	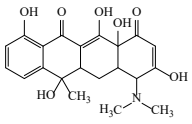	$C_{21}H_{23}NO_7$	401.42	401
9	2,3,4a,5,7,11-hexahydroxy-11-methyl-2,3,11,11a,12,12a-hexahydrotetracene-1,4,6(4a*H*)-trione	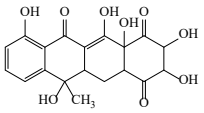	$C_{19}H_{18}O_9$	390.34	391
10	(*E*)-4-hydroxy-4-((*Z*)-4,8a,9a-trihydroxy-4-methyl-1,3,5,6,7,8,9-heptaoxododecahydroanthracen-2(1*H*)ylidene)but-2-enoic acid	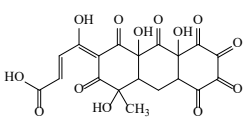	$C_{19}H_{14}O_{13}$	450.31	451

11	2,5,8a,9a-tetrahydroxy-5-methyl-1,3,4,6,7,8,9-heptaoxotetradecahydro-anthracene-2-carboxylic acid	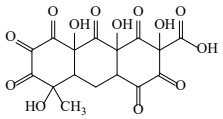	$C_{16}H_{12}O_{13}$	412.26	413
12	1,2,8,10-tetrahydroxy-2-(2-hydroxya-cetyD)-3-(2-hydroxyethyl)-3,4,4a,10-tetrahydroanthracen-9(2*H*)-one	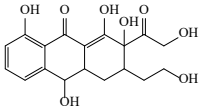	$C_{18}H_{20}O_8$	364.35	365
13	4a,10a-dihydroxy-8-methyltetrahydro-anthracen-1,2,3,4,5,6,7,10(4a*H*,8*H*)-oc-taone	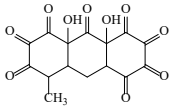	$C_{15}H_{10}O_{10}$	350.24	349
14	3-(1-amino-3-hydroxy-2-oxopropyl)-1,2,8-trihydroxy-10-methyl-3,4,4a,10-tetrahydroanthracen-9(2H)-one	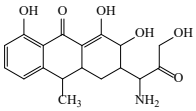	$C_{18}H_{21}NO_6$	347.37	347
15	4,5-dihydroxy-9-methyl-10-oxo-1,2,3,9,9a,10-hexahydroanthracene-2,3-dicarboxylic acid	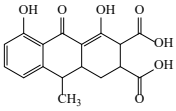	$C_{17}H_{16}O_7$	332.31	332
16	1,8-dihydroxy-3-(hydroxymethyl)-10-methyl-9-oxo-2,3,4,4a,9,10-hexahydro-anthracene-2-carboxylic acid	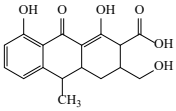	$C_{17}H_{18}O_6$	318.33	317
17	1,8,9a-trihydroxy-10-methyl-9-oxo-1,2,3,4,4a,9,9a,10-octahydroanthra-cene-2-carboxylic acid	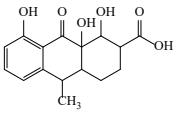	$C_{16}H_{18}O_6$	306.31	306
18	1,8-dihydroxy-9-oxo-2,3,4,4a,9,10-hex-ahydroanthracene-2-carboxylic acid	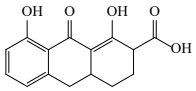	$C_{15}H_{14}O_5$	274.27	274
19	4a-hydroxynaphthalene-1,2,3,4,5,6,7(4aH)-heptaone	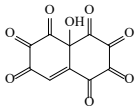	$C_{10}H_2O_8$	250.12	250
20	1-hydroxy-3,4,5,6-tetraoxocyclohexane-1,2-dicarboxylic acid	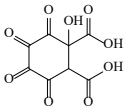	$C_8H_4O_9$	244.11	245
21	7,8a-dihydroxy-7-(hydroxymethyl) hex-ahydronaphthalene-1,2,8(5H)-trione	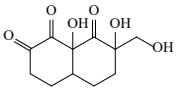	$C_{11}H_{14}O_6$	242.23	242
22	1-hydroxy-4,5,6-trioxocyclohexane-1,2-dicarboxylic acid	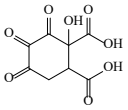	$C_8H_6O_8$	230.13	230
23	2-acetyl-8-hydroxy-4-methyl-3,4-dihy-dronaphthalen-1(2H)-one	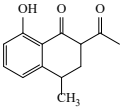	$C_{13}H_{14}O_3$	218.25	218
24	3,4,5-trioxocyclohexane-1,2-dicarbox-ylic acid	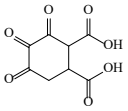	$C_8H_6O_7$	214.13	213

25	1,6-dihydroxycyclohex-4-ene-1,2-dicarboxylic acid	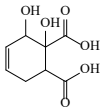	$C_8H_{10}O_6$	202.16	203
26	1,6-dihydroxycyclohexa-2,4-diene-1,2-dicarboxylic acid	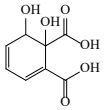	$C_8H_8O_6$	200.15	201
27	3-hydroxycyclohexa-2,4-diene-1,2-dicarboxylic acid	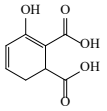	$C_8H_8O_5$	184.15	185
28	1,2-dihydroxyethane-1,1,2,2-tetracarboxylic acid	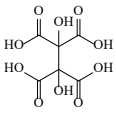	$C_6H_6O_{10}$	238.10	239
29	1-hydroxyethane-1,1,2,2-tetracarboxylic acid	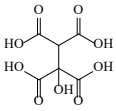	$C_6H_6O_9$	222.11	223
30	1-hydroxyethane-1,1,2-tricarboxylic acid	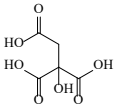	$C_5H_6O_7$	178.10	178
31	2,3-dihydroxyfumaric acid	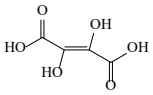	$C_4H_4O_6$	148.07	149
32	2-oxomalonic acid	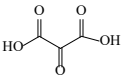	$C_3H_2O_5$	118.04	118
33	2,3-dioxopropanoic acid		$C_3H_2O_4$	102.05	101
34	oxalic acid		$C_2H_2O_4$	90.03	90
35	acrylic acid	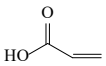	$C_3H_4O_2$	72.06	71
36	formic acid		CH_2O_2	46.03	45

56

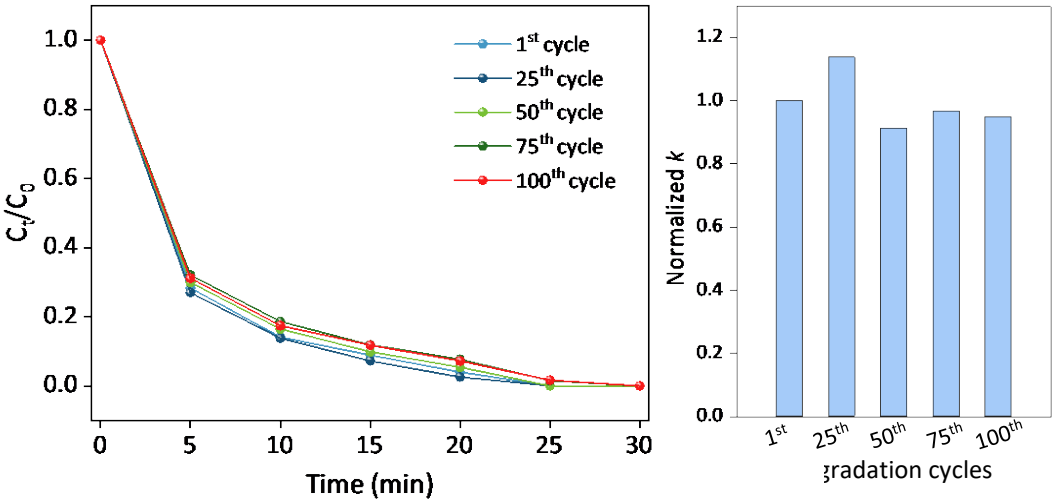

Fig. S4. Long-term stability test. (a) Removal rate collected from the 1st, 25th, 50th, 75th and 100th cycle individually. (b) the corresponding pseudo-first-order reaction rate constants. Repetitive degradation test was performed with a current of 0.2 A for 30 min and the reactor was under constant stirring at a speed of 300 rpm. The solution contains an electrolyte of 50 mM Na_2SO_4, the catalyst of 20 mM persulfate and 0.05 mM Fe^{2+}, and a degradation analyte of 0.1 mM tetracycline. The oxygen gas was supplemented by pumping air with a flow rate of 0.25 L min^{-1}. The solution pH and temperature maintained at 7 and 20 °C throughout the experiments.

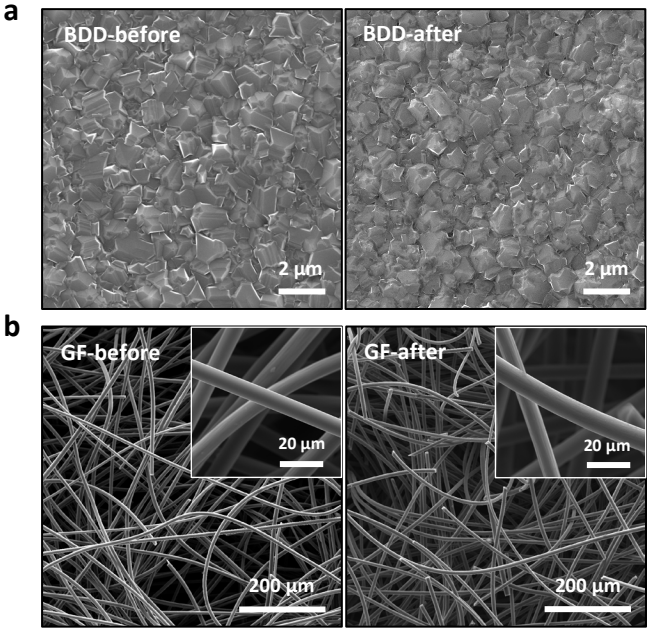

Fig. S5. Scanning electron morphologies of (a) BDD anode and (b) GF cathode before and after 100-cycle degradation experiments.

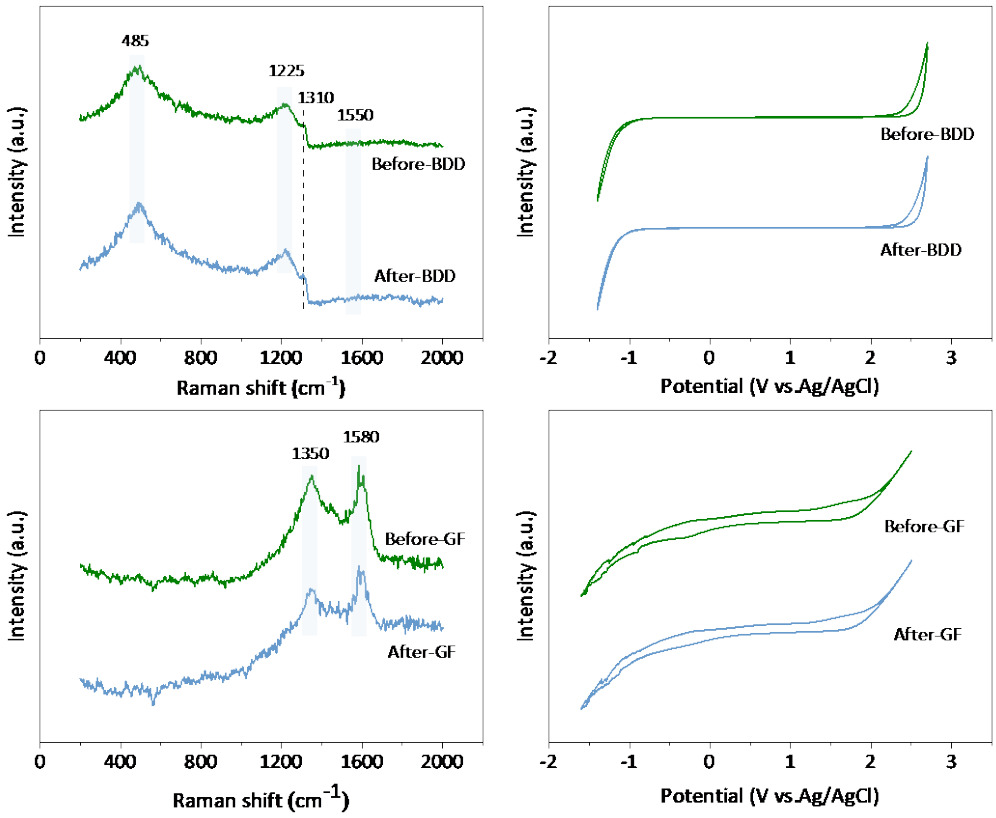

Fig. S6. (a, c) Raman spectra and (b, d) Cyclic voltammograms in 0.5 M H_2SO_4 of BDD anode and GF cathode before and after water treatment.

Table S5

Comparison of the EO-PS-EF method with the reported AOPs for the degradation of TC.

Methods	Pollutants	Operating conditions	Pollutant removal	Energy consumption	Ref.
Sonocatalytic oxidation	Tetracycline	10 mg L^{-1} TC, 0.25 L, 500 W, 1 g L^{-1} BiOBr/$FeWO_4$, pH 6.5	91.2% in 30 min	2500 kWh m^{-3}	(Xu et al., 2023)
3D Electro-Fenton	Tetracycline	50 mg L^{-1} TC, 0.1 L, 6.66 mA cm^{-2}, 10 mM NaCl, 0.5 g L^{-1} MMC/Fe_3O_4	100% in 20 min	43 kWh m^{-3} (0.86 kWh g^{-1} TC)	(Alizadeh et al., 2023)
Electro-Fenton	Tetracycline	60 mg L^{-1} TC, 0.2 L, 0.2 A, 0.5 mM Fe^{2+}, pH 2.8, 50 mM Na_2SO_4, NAC-1100/GF cathode	83.1% in 120 min	13.83 kWh m^{-3}(230.44 kWh kg^{-1} TC)	(Han et al., 2022)
Electrochemical oxidation	Tetracycline	0.2 mM TC, 0.08 L, 0.1 A, 25 mM Na_2SO_4, pH 2, Ru-coated graphite anode	93.8% in 100 min	10.04 kWh m^{-3}	(Köktaş et al., 2023)
Piezocatalytic oxidation	Tetracycline	20 mg L^{-1} TC, 0.2 L, 200 mg Fe_3O_4@MoS_2/PVDF pipe, water flow driving	92.5% in 100 min	241.04 kWh m^{-3} $order^{-1}$	(Wang et al., 2023)
Electrochemical oxidation	Tetracycline	50 mg L^{-1} TC, 0.15 L, 10 mA cm^{-2}, 0.075 M Na_2SO_4	90% in 60 min	2.84 kWh m^{-3} $order^{-1}$	(Pang et al., 2021)
Photocatalytic oxidation	Tetracycline	10 mg L^{-1} TC, 0.1 L, 300 W, 0.03 g 12 % $ZnFe_2O_4$/Bi_2S_3	91.6% in 120 min	2.57 kWh m^{-3} $order^{-1}$	(Yan et al., 2023)
Electrochemical oxidation-Persulfate-$MnFe_2O_4$	Tetracycline	25 mg L^{-1} TC, 0.1 L, 20 mA cm^{-2}, 0.2 g L^{-1} $MnFe_2O_4$, 2 mM PS, pH 4.5	86.2% in 60 min	2.33 kWh m^{-3} $order^{-1}$	(Tang et al., 2021b)
Electrochemical oxidation-Fe_3O_4-Peroxydisulfate	Tetracycline	25 mg L^{-1} TC, 0.1 L, 20 mA cm^{-2}, 0.2 g L^{-1} Fe_3O_4, 2 mM PDS, pH 4.5	86.5% in 60 min	2.02 kWh m^{-3} $order^{-1}$	(Tang et al., 2021a)
EO-PS-EF	Tetracycline	0.1 mM TC, 0.25 L, 50 mA cm^{-2}, 20 mM PS, 0.05 mM Fe^{2+}, 0.25 L min^{-1} Air, pH 7	100% in 30 min	1.65 kWh m^{-3} (0.42 kWh m^{-3} $order^{-1}$)*	This work

Note: *Energy consumption (kWh m^{-3} $order^{-1}$) proposed by the International Union of Pure and Applied Chemistry is used to calculate the energy required for pollutant degradation (Wang et al., 2023).

References

Alizadeh, Z., Jonoush, Z.A. and Rezaee, A. 2023. Three-dimensional electro-Fenton system supplied with a nanocomposite of microbial cellulose/Fe_3O_4 for effective degradation of tetracycline. Chemosphere 317, 137890.

Han, S., Wang, Z., Pi, X., Wu, C., Wang, X., Wang, Y., Liu, X. and Zhao, H. 2022. Promotion of tetracycline degradation by electro-Fenton: Controlling the reaction zone by N-doped modified activated carbon cathode. J. Clean. Prod. 370, 133524.

Köktaş, İ.Y., Gökkuş, Ö., Kariper, İ.A. and Othmani, A. 2023. Tetracycline removal from aqueous solution by electrooxidation using ruthenium-coated graphite anode. Chemosphere 315, 137758.

Pang, D., Liu, Y., Song, H., Chen, D., Zhu, W., Liu, R., Yang, H., Li, A. and Zhang, S. 2021. Trace Ti^{3+}- and N-codoped TiO_2 nanotube array anode for significantly enhanced electrocatalytic degradation of tetracycline and metronidazole. Chem. Eng. J. 405, 126982.

Tang, S., Zhao, M., Yuan, D., Li, X., Wang, Z., Zhang, X., Jiao, T. and Ke, J. 2021a. Fe_3O_4 nanoparticles three-dimensional electro-peroxydisulfate for improving tetracycline degradation. Chemosphere 268, 129315.

Tang, S., Zhao, M., Yuan, D., Li, X., Zhang, X., Wang, Z., Jiao, T. and Wang, K. 2021b. $MnFe_2O_4$ nanoparticles promoted electrochemical oxidation coupling with persulfate activation for tetracycline degradation. Sep. Purif. Technol. 255, 117690.

Wang, J., Zhou, X., Hao, J., Wang, Z., Huo, B., Qi, J., Wang, Y. and Meng, F. 2023. Sustainable self-powered degradation of antibiotics using Fe_3O_4@MoS_2/PVDF modified pipe with superior piezoelectric activity: Mechanism insight, toxicity assessment and energy consumption. Appl. Catal. B: Environ. 331, 122655.

Xu, L., Wu, X.-Q., Li, C.-Y., Liu, N.-P., An, H.-L., Ju, W.-T., Lu, W., Liu, B., Wang, X.-F., Wang, Y. and Wang, X. 2023. Sonocatalytic degradation of tetracycline by BiOBr/$FeWO_4$ nanomaterials and enhancement of sonocatalytic effect. J. Clean. Prod. 394, 136275.

Yan, B., Peng, J., Deng, F., Liu, L., Li, X., Shao, P., Zou, J., Zhang, S., Wang, J. and Luo, X. 2023. Novel $ZnFe_2O_4$/Bi_2S_3 high-low junctions for boosting tetracycline degradation and Cr(VI) reduction. Chem. Eng. J. 452, 139353.